Rhie–Chow interpolation.[5] From Fig. 1, it is seen that the pressure oscillations resulting from the original Rhie–Chow interpolation are most pronounced at small time steps. To quantify the size of the deviations and oscillations, the following two quantities are computed:

$$\text{deviation} = \frac{1}{V}\int_V (s_{\text{RC}} - s_{\text{New}})\,\mathrm{d}v \tag{12}$$

$$\text{oscillation} = \frac{1}{V}\int_V \left(\delta_x^2 + \delta_y^2\right)(s_{\text{RC}} - s_{\text{New}})\,\mathrm{d}v \tag{13}$$

where s_{RC} and s_{New} are the solutions computed with the original Rhie–Chow scheme and the new scheme, respectively. The new scheme gives the same solution independent of the time step. Table 1 shows the deviation and oscillation for different time steps. From Table 1, the deviations are almost independent of the time step (from 0.01 to 0.001). The oscillations, however, become more important at decreasing time steps.

B. Unsteady Solution at a Reynolds Number of 200

The flow past a circular cylinder at Reynolds number of 200 is computed with a time step $\delta t = 0.0025$. After a dimensionless time of 200, corresponding to 80,000 time steps, a periodic solution is reached.

Figure 2 shows pressure contours computed with the modified and the original interpolation schemes. From Fig. 2, oscillations are clearly visible for the original Rhie–Chow interpolation,[5] whereas the modified interpolation displays no oscillations. For the force coefficients, the new interpolation gives almost the same values as the original interpolation scheme, except that the mean value of C_D is increased with about 0.25%.

IV. Conclusions

The origin of pressure oscillations produced by the Rhie–Chow procedure[5] when running at small time steps has been revealed. A revised procedure for the interpolation of cell face fluxes is proposed. Oscillations are succesfully eliminated by the revised procedure. The new interpolation scheme contributes no extra dissipation as compared to the Rhie–Chow procedure. The revised procedure is consistent for all time step lengths and can be used for other methods based on collocated grids, for example, the fractional step method.

References

[1]Patankar, S. V., *Numerical Heat Transfer and Fluid Flow*, Hemisphere, New York, 1980, Chap. 6.

[2]Akselvoll, K., and Moin, P., "An Efficient Method for Temporal Integration of the Navier–Stokes Equations in Confined Axisymmetric Geometries," *Journal of Computational Physics*, Vol. 125, No. 2, 1996, pp. 454–463.

[3]Karki, K. C., and Patankar, S. V., "Pressure-Based Calculation Procedure for Viscous Flows at All Speeds in Arbitrary Configurations," *AIAA Journal*, Vol. 27, 1989, pp. 1167–1174.

[4]Rubin, S. G., and Harris, J. E., "Numerical Studies of Incompressible Viscous Flow in a Driven Cavity," NASA SP-378, 1975.

[5]Rhie, C. M., and Chow, W. L., "Numerical Study of the Turbulent Flow Past an Airfoil with Trailing-Edge Separation," *AIAA Journal*, Vol. 21, No. 11, 1983, pp. 1525–1532.

[6]Majumdar, S., "Role of Underrelaxation in Momentum Interpolation for Calculation of Flow with Nonstaggered Grids," *Numerical Heat Transfer*, Vol. 13, No. 1, 1988, pp. 125–132.

[7]Ferziger, J. H., and Peric, M., *Computational Methods for Fluid Dynamics*, Springer-Verlag, Berlin, 1996, Chap. 8.

[8]Michelsen, J. A., "Basis3D—A Platform for Development of Multiblock PDE Solvers," Technical Univ. of Denmark, AFM 92-05, Lyngby, Denmark, 1992.

[9]Sørensen, N. N., "General Purpose Flow Solver Applied over Hills," Risø National Lab., RISØ-R-827-(EN), Roskilde, Denmark, 1995.

R. M. C. So
Associate Editor

Side Force on an Ogive Cylinder: Effects of Freestream Turbulence

S. C. Luo,* K. B. Lua,† and T. T. Lim*
National University of Singapore, Singapore 119260, Republic of Singapore
and
E. K. R. Goh‡
DSO National Laboratories, Singapore 118230, Republic of Singapore

Nomenclature

b	=	grid bar diameter
Cy	=	side-force coefficient, $F_y/(0.5\rho U_\infty^2 S)$
Cy_D	=	local side-force coefficient, local side force/$(0.5\rho U_\infty^2 D \sin^2\alpha)$
D	=	cylinder diameter
Fy	=	side force
I	=	turbulence intensity; I_x is the longitudinal turbulence intensity in freestream direction, σ_x/U
L	=	turbulence length scale; L_x is the longitudinal turbulence length scale in the freestream direction
M	=	mesh-opening length
P	=	pressure on model surface
P_∞	=	freestream static pressure
R	=	autocorrelation coefficient
Re_D	=	Reynolds number, $U_\infty D/\nu$
S	=	model base area, $\pi D^2/4$
T	=	timescale
U	=	time-averaged freestream velocity
X	=	axial distance from model nose tip
x	=	distance downstream from the grid
α	=	angle of attack
θ	=	azimuth angle around circular cross section measured from the most leeward position
ν	=	kinematics viscosity of fluid
ρ	=	density of fluid
σ_x	=	standard deviation of the freestream velocity
τ	=	time difference
ϕ	=	roll angle

Introduction

FREESTREAM turbulence is known to affect the side force acting on ogive cylinders pitched at high angles of attack for many years. For instance, Lamont and Hunt[1] found in their investigation that freestream turbulence caused the switching of the asymmetric flow states, resulting in a substantially smaller time-averaged side force. This finding was supported by Hunt and Dexter,[2] who conducted a study that included both high and low turbulence intensities ($I_x = 0.7$–0.01%) and found that the switching has disappeared in a "quieter" environment. In a later study Howard et al.,[3] who used four turbulence generating grids to modify freestream turbulence intensity and length scale, also found that increased turbulence intensity substantially reduced the maximum induced side force. However, not everyone seems to agree with the preceding findings. Wardlaw

Received 14 July 2000; revision received 14 December 2000; accepted for publication 19 March 2001.

*Associate Professor, Department of Mechanical Engineering, 10 Kent Ridge Crescent.
†Research Engineer, Department of Mechanical Engineering, 10 Kent Ridge Crescent.
‡Senior Member of Technical Staff, 20 Science Park Drive.

and Yanta[4] found that by increasing the turbulence intensity to about 2% the peaks of side force distributions is increased by about 10%.

These contradictory results raise a pertinent question: How does freestream turbulence modify the side force on a slender body? The desire to address the preceding question motivated us to carry out the present investigation: to study the effects of freestream turbulence on the side force acting on an ogive cylinder at high incidence experimentally via simultaneous side-force and surface-pressure measurements. Five grids were installed (one at a time) at various locations in the wind tunnel to generate turbulence. By selecting grid of the appropriate size and adjusting its upstream location from the model, we were able to vary the turbulence length scale while ensuring that the turbulence intensity is constant and vice versa. In contrast to many of the previous studies, which were restricted to only one or a few roll angles, the present investigation covers one complete rotation of the model, with the side-force and surface-pressure measurements measured at a roll angle interval of 7.2 deg. We believe that the finely mapped-out results of side force and surface pressure can give us a better insight into how freestream turbulence affects the side-force distribution.

Experimental Apparatus and Techniques

The experiments were carried out in an open-loop suction wind tunnel with a rectangular cross section measuring 0.6 m(H) × 1.0 m(W). The ogive cylinder used in the present study is the same as the one used in our earlier study.[5] All of the measurements were conducted at a freestream velocity U of 15m/s, and the Reynolds number Re_D based on the diameter ($D = 35$ mm) of the cylindrical section of the model is about 3.5×10^4. At this operating condition the boundary layer involved was laminar because Lamont[6] has shown that boundary layer remains laminar below $Re_D = 2 \times 10^5$ for all angles of attack. The turbulence intensity of the empty wind tunnel is about 0.23%.

Five sets of biplanar square-mesh grids were used in the present investigation, in all cases the ratio of the grid opening M to bar diameter b was fixed at $M/b = 5$. The purpose of using grids of different sizes is to enable us to vary the turbulence length scale because it is proportional to the grid opening. To establish a reasonably good isotropic turbulence flow condition, a distance of 5–10 mesh size (i.e., 5–10M) downstream of the screen is required. To meet this condition, all of the present measurements were conducted at least 15 mesh-size downstream of the grid. The constant temperature hot-wire anemometry (CTA) was used to measure the x-(flow) direction turbulence intensity I_x, the autocorrelation coefficient R, and the turbulence length scale L_x. A 5μ-diam tungsten wire with a sensing length of 1.2 mm was used throughout the experiment. The CTA unit was linked to a PC via a data acquisition system. In the calculation of the integral timescale T, only the area under the positive part of the correlation curve in the R–τ plot was considered for the data reduction.

Figure 1 defines the sign convention used for the side force, the roll direction of the model (ϕ) and the azimuth angle (θ). Here, the positive side force is always pointed toward the starboard side of the body (i.e., in the positive y direction of the coordinates system that is fixed with respect to the wind tunnel). The zero azimuth angle is always located at the most leeward position, and the azimuth angle increases in a counterclockwise direction (when viewed from the top). The azimuth angle is also fixed with respect to the wind tunnel.

To measure the changes in the side force with the roll angle, the model was rotated in a counterclockwise direction by a software-controlled stepper motor located at the back of the model, just below the floor of the wind-tunnel test section. Both the model and the stepper motor were subsequently mounted on an inclined mechanism sitting on a Nitta six-degree-of-freedom force balance. The accuracy of the balance is ±1.16 gm, which corresponds to a maximum error of ±0.0891 in the side-force coefficient Cy at the operating speed of 15 m/s.

A computer equipped with a Pentium II microprocessor was used to both acquire the data and control the stepper motor. During a typical data acquisition routine, after the model had been rotated by the stepper motor to a new roll angle, a 2-s delay was allowed for the flow to stabilize before force measurements were taken at a sampling frequency of 1 kHz over 10 s. This was then followed by pressure measurements of all the 76 pressure tapings, with 5000 data collected at each pressure tap at a sampling frequency of 1 kHz. Because of the limitation of the data acquisition card, pressure measurements had to be carried out in a sequential manner using two sets of scanivalve. After the completion of the data acquisition, all of the results were time averaged and stored in a hard disk before the model was rotated to the next roll angle. The preceding process was then repeated. Measurements were carried out over the entire 360-deg roll-angle range at an interval of 7.2 deg.

Results and Discussion

The present study is made up of two parts. In the first part the length-scale L_x/D is kept constant at either 0.354, 0.428, or 0.575, while the turbulence intensity I_x is varied from 1.2 to 3.9%. In the second part the intensity level is kept constant either at 1.9, 2.9, or 3.9%, while the turbulence length scale is varied from 0.252 to 0.569. In all cases the ogive cylinder is pitched at an angle of attack α of 50 deg. This angle is chosen based on our earlier investigation on the same cylinder, which showed that $\alpha = 50$ deg gives the maximum side force, and the available surface-pressure tappings cover at least the first local side-force peak.[5]

The results when the turbulence length scale L_x/D was fixed at 0.354 and the I_x varied from 1.2 to 3.4% are shown in Fig. 2 as a typical set of results on the effects of the turbulence intensity. It is clear from the figure that the turbulence intensity has significant influence on the side-force distribution. With the benefit of the hindsight that the model's surface condition is unlikely to be completely uniform, it is perhaps not surprising to see that different parts of the model respond differently to turbulence intensity. In the case of the present wind-tunnel model and the way it was set up, the roll angle range of $180 < \phi < 270$ deg seems to be the most affected, with the side force decreasing with increasing turbulence intensity. This is what Lamont and Hunt and Howard et al. found in their investigations. However, outside the preceding range of roll angle, there is a small but noticeable increase in the side force when the turbulence intensity increases. This agrees with what Wardlaw and Yanta reported in their investigation. The present results therefore suggest that the contradiction among different results reported in the literature is caused by differences in model surface conditions.

To obtain a better insight into the flow characteristics just discussed, Fig. 3 shows the local side-force distribution along the axial

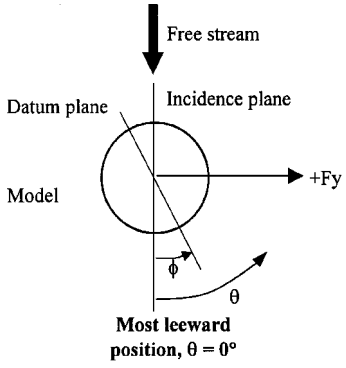

Fig. 1 Definitions of side force Fy, roll angle ϕ, and azimuth angle θ.

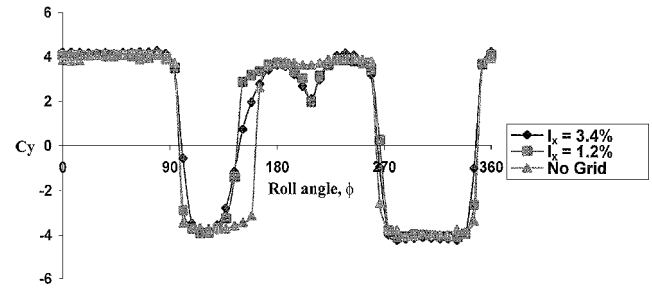

Fig. 2 Effects of varying turbulence intensity I_x when turbulence length scale L_x/D is kept constant at 0.354.

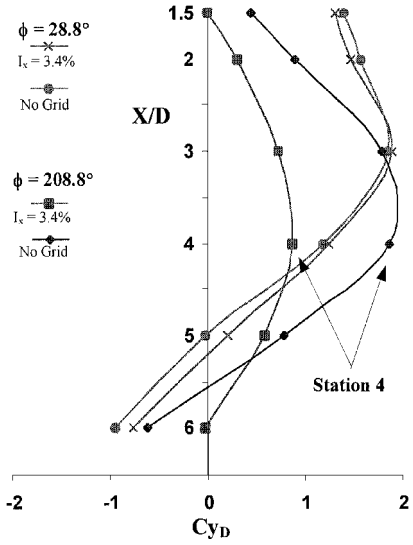

Fig. 3 Local side-force distributions in the model axial direction when no grid was installed and when $I_x = 0.034$; $\phi = 28.8$ and 208.8 deg.

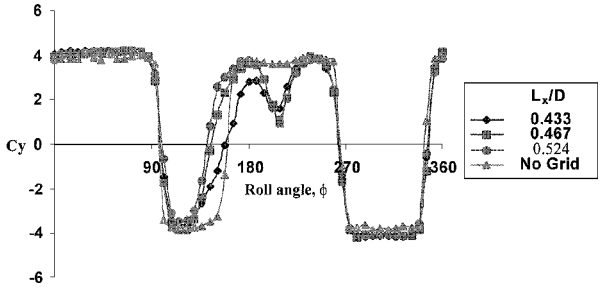

Fig. 4 Effects of varying the turbulence length scale L_x when turbulence intensity I_x is kept constant at 3.9%.

direction of the model for cases with and without the presence of the grids. The local side force Cy_D is obtained by integrating the local surface-pressure measurements. Using the results of the turbulence intensity $I_x = 3.4\%$ as an example, it can be seen that at $\phi = 28.8$ deg there is only a very small difference in the local side-force distribution between the relatively smooth (no grid installed) and the turbulent ($I_x = 3.4\%$) flow. This is consistent with the total side-force data shown in Fig. 2. However at $\phi = 208.8$ deg, where there is a large "dip" in the overall side-force distribution in Fig. 2, the turbulence intensity has certainly caused a substantial reduction in the local side force.

We next study the effects of turbulence length scale while keeping the turbulence intensity constant, and the results for the fixed turbulence intensity I_x of 3.9% are shown in Fig. 4. Unfortunately, because of the relatively small range in L_x/D used (0.433–0.524), no clear trend in the change of the side-force distribution with variation in the turbulence length scale can be detected. For the present results the smallest length scale of $L_x/D = 0.433$ appears to have the greatest influence in reducing side force in virtually all cases when $\phi = 208.8$ deg (the approximate roll angle where the greatest side-force reduction takes place). It is believed that a larger range of L_x/D is needed before its effects on the side force can be fully appreciated, and more systematic work is obviously required.

Conclusions

The effects of freestream turbulence on the side force acting on an ogive cylinder at high angle of attack have been studied experimentally over a range of turbulence intensity and length scale. By carefully locating the positions of the turbulence generating grids upstream of the cylinder, the turbulence intensity was varied independently of the turbulence length scale and vice versa.

Side-force and surface-pressure measurements clearly show that, for a fixed angle of attack, an increase in the turbulence intensity can cause the side force to either decrease or increase, depending on the roll-angle position (surface conditions) of the cylinder. This explains the sometimes contradictory findings reported in the literature. As for the turbulence length scale, it also appears to have influence on the cylinder's side force, but because of the relatively small L_x/D range used no clear trend was detected. In the present case the smallest $L_x/D (= 0.433)$ appears to have the greatest influence in reducing side force. More systematic investigation is needed in this area.

References

[1]Lamont, P. J., and Hunt, B. L., "Pressure and Force Distributions on a Sharp-Nosed Circular Cylinder at High Angles of Inclination to a Uniform Subsonic Stream," *Journal of Fluid Mechanics*, Vol. 76, No. 3, 1976, pp. 519–559.

[2]Hunt, B. L., and Dexter, P. C., "Pressure on a Slender Body at High Angle of Attack in a Very Low Turbulence Level Air Stream," CP 247, AGARD, Oct. 1978.

[3]Howard, R. M., Rabang, M. P., and Roane, D. P., Jr., "Aerodynamic Effects of a Turbulent Flowfield on a Vertically Launched Missile," *Journal of Spacecraft*, Vol. 26, No. 6, 1989, pp. 445–451.

[4]Wardlaw, A. B., and Yanta, W. J., "Multistable Vortex Patterns on Slender, Circular Bodies at High Incidence," *AIAA Journal*, Vol. 20, No. 4, 1982, pp. 509–515.

[5]Luo, S. C., Lim, T. T., Lua, K. B., Chia, H. T., Goh, E. K. R., and Ho, Q. W., "Flowfield Around Ogive/Elliptic-Tip Cylinder at High Angle of Attack," *AIAA Journal*, Vol. 36, No. 10, 1998, pp. 1778–1787.

[6]Lamont, P. J., "Pressure Around an Inclined Ogive Cylinder with Laminar, Transitional, or Turbulent Separation," *AIAA Journal*, Vol. 20, No. 11, 1982, pp. 1492–1499.

A. Plotkin
Associate Editor

Turbulence in Wake of a Self-Propelled Body with and without Swirl

A. I. Sirviente*
University of Michigan, Ann Arbor, Michigan 48109-2145
and
V. C. Patel†
University of Iowa, Iowa City, Iowa 52242-1585

I. Introduction

In the wake of a self-propelled body, the drag of the body is matched by the thrust developed by the propulsion device, and there is no net momentum flux. Measurements in such a momentumless wake of a bluff axisymmetric body propelled by a jet, without[1] and with swirl,[2] were recently made to document the turbulent mixing in the near field and study evolution of the wake. Measurements were also made in so-called component flows, namely the drag wake[3] of the body without propulsion and an isolated nonswirling jet and a swirling jet issuing from the base of the body. The previous publications reported the streamwise development of the momentumless wake, without[1] and with swirl.[2] This development takes place in three stages: the near field, in which the body boundary layer and the jet are clearly evident; an intermediate region, in which the two flows mix up to the axis of the body; and last the

Received 20 December 2000; revision received 30 August 2001; accepted for publication 5 September 2001.

*Assistant Professor, Department of Naval Architecture and Marine Engineering. Member AIAA.

†Director and Professor, Iowa Institute of Hydraulic Research and Department of Mechanical Engineering. Associate Fellow AIAA.